RSC Applied Polymers

ROYAL SOCIETY OF CHEMISTRY

PAPER

View Article Online
View Journal | View Issue

Cite this: *RSC Appl. Polym.*, 2024, **2**, 936

Cellulosic protic ionic liquid hydrogel confined Pd nanoparticles for selective hydrogenation of α-angelica lactone and alkenes

Tonghui Xu, Xianyi Zhu, Kui Chen, Tianlong He, Lihua Zhang, Jili Yuan and Haibo Xie *

Hydrogenation is one of the important functional group conversion reactions in the chemical industry. In this study, a cellulosic protic ionic liquid hydrogel was firstly synthesized by adding mixed cyclic anhydrides into a cotton pulp cellulose solution in TMG (1,1,3,3-tetramethyl guanidine)/CO_2/DMSO to form the cellulosic protic ionic liquid hydrogel (CPILH) through an esterification reaction. The CPILH confined Pd nanoparticle (Pd@CPILH) catalyst was prepared by anchoring Pd^{2+} ions through the large functional groups on the CPILH (*e.g.*, –COOH and TMG-based protic ionic liquids (TMGPILs)) and then an *in situ* reduction of Pd^{2+} to Pd NPs. TEM analysis revealed that the Pd NPs had a small size of 4.4 nm and were well dispersed within the matrix. As a result, catalytic hydrogenation of α-AL successfully formed GVL, with a conversion rate of 97.7% and 100% selectivity achieved within 3 hours at 50 °C in ethanol. Kinetics experiments were performed by adjusting the reaction temperature within the range of 30 to 65 °C, and the simulated data fitted well with the first-order kinetic law. The reaction rate constant (k) was determined to be 0.2226 min^{-1} at 50 °C, and the reaction activation energy (E_a) was calculated to be 30.45 kJ mol^{-1}. The Pd@CPILH catalyst demonstrated remarkable recyclability, maintaining high conversion and selectivity even after 10 uses. Additionally, the catalyst exhibited excellent catalytic efficiency, achieving nearly 100% conversion and selectivity for common alkenes under moderate conditions. This work presents a straightforward and sustainable strategy for the synthesis of catalyst support materials, showcasing significant potential in the production of chemicals derived from biomass.

Received 3rd May 2024,
Accepted 7th July 2024

DOI: 10.1039/d4lp00150h

rsc.li/rscapplpolym

Introduction

Lignocellulosic biomass emerges as a promising, abundant, biorenewable, and cost-effective feedstock for the synthesis of diverse bio-based chemicals and materials.[1,2] Typically, γ-valerolactone (GVL) is a well-known biobased chemical from lignocellulosic biomass owing to its attractive properties. GVL exhibits favorable physicochemical characteristics, including low toxicity and biodegradability, rendering it an excellent choice for applications as a green solvent, perfume, and fuel additive.[3–9] In addition to its aforementioned properties, GVL has been recognized as a versatile platform chemical with the capability to generate a collection of high added-value chemicals,[10,11] such as methyltetrahydrofuran,[12] alkanes,[13] 1,4-pentanediol,[14] 2-methyltetrahydrofuran,[15] methyl valerate,[16] adipic acid,[17] and biobased polymers.[18] Therefore, many studies have reported numerous methods for the preparation of GVL.

At present, significant progress has been made in the research of synthesizing GVL. Zhang *et al.* prepared a series of NiO/SiO_2 carriers with different Ni contents by wet impregnation using $Ni(NO_3)_2$ as a precursor and then calcination in air. A small amount of palladium (0.2 wt%) was then upsampled by deposition reduction ($NaBH_4$ as the reducing agent) and α-angelicoside liquid-phase hydrogenation to γ-valerolactone (GVL) under mild conditions.[19] But the catalyst preparation is relatively complex and costly. Antunes *et al.* utilized a nanohybrid catalyst (M-FDCA) to convert α-angelica lactone (α-AL) to GVL, revealing the multifunctional behavior of the hybrid catalysts in a one-pot conversion of α-AL to GVL involving both acid and reduction chemistry.[20] Recent studies have demonstrated that supported metal catalysts, such as Pd/C, $Pd/NiO/SiO_2$, and M-FDCA (M = Zr or Hf) catalysts, could promote the hydrogenation reaction and facilitate the conversion of α-AL into GVL.[21–24] Unfortunately, these reports often involved high H_2 pressure (>1 MPa) and elevated reaction temperatures (150 °C–180 °C), or required high-temperature calcination for the preparation of support materials to anchor

Department of Polymeric Materials & Engineering, College of Materials & Metallurgy, Guizhou University, West Campus, Guizhou University, Huaxi District, Guiyang, 550025, P. R. China. E-mail: hbxie@gzu.edu.cn

the Pd-related catalyst. Although these conditions resulted in relatively higher yields and selectivity for the hydrogenation process, there is a need to design a more convenient method for preparing support materials that can effectively anchor Pd. This would enable efficient and mild production of GVL using α-AL as the starting material.

Among various support materials, hydrogels have obtained particular attention in catalysis applications as their three-dimensional and porous structure not only offers good accommodation for metal nanoparticles but also provides channels for the transport of reaction reagents and products.[25] The utilization of natural polymers for the fabrication of hydrogel matrices has garnered considerable attention, with cellulose-based hydrogels standing out as a particularly noteworthy choice. The key factors driving this interest include the abundance, renewability, non-toxic nature, and biodegradability of cellulose-based hydrogels.[26,27] Additionally, the structural characteristics of cellulose, which contains numerous hydroxyl groups in its polymer chains, presents exciting possibilities for incorporating specific functional groups into advanced cellulosic materials. For example, a cellulose hydrogel was cross-linked through epichlorohydrin in the NaOH/urea system, and copper nanoparticles were *in situ* loaded on the cellulose hydrogel for the reduction of 4-nitrophenol.[28] In our previous study, a carboxylcellulose hydrogel was designed as a matrix material to confine Fe_3O_4 nanoparticles for Fenton-like catalysis of rhodamine B decoloration.[29] Additionally, we demonstrated the exceptional immobilization and stabilization capabilities of a cellulosic hydrogel functionalized with TMG based protic ionic liquids for Pd NPs. This resulted in a highly efficient catalytic performance in the hydrogenation of 4-nitrophenol, achieving a turnover frequency (TOF) of 25.14 h^{-1}.[30] Our research reveals that these favorable application performances are ascribed to the structural features of the cellulosic protic ionic liquid hydrogel (CPILH); not only does it permit homogeneous dispersion and stabilization of metal NPs, but it also provides connected porous channels enabling the catalytic process to proceed rapidly. Therefore, it is perfectly capable as a carrier for Pd NPs in the field of catalytic hydrogenation of α-AL to produce GVL.

Herein, we synthesized the CPILH by introducing cyclic anhydride into an innovative cellulose solution in TMG/CO_2/DMSO, resulting in the formation of a cellulosic protic ionic liquid hydrogel through an esterification reaction. Based on the strategy for CPILH structure design, a significant number of functional groups (*e.g.*, TMGPILs and –COOH) were suspended on the cellulose backbone by the one-pot method. This resulted in a three-dimensional and porous CPILH with abundant metal NPs ligand sites, enabling the anchoring of Pd NPs *via* N-element coordination. Consequently, the Pd@CPILH catalyst that we prepared exhibited high catalytic hydrogenation and exceptional reusability for α-LA to GVL conversion. Furthermore, we observed that Pd@CPILH also demonstrated excellent catalytic performance for typical alkene hydrogenation. These findings provide a promising approach for developing environmentally friendly hydrogel support materials. These materials have immense potential for use in green catalysis and chemical engineering, underscoring their significance in advancing sustainable practices.

Materials and methods

Materials

Cotton pulp cellulose (DP = 359) was subjected to vacuum drying at 60 °C for 24 h prior to usage. 1,1,3,3-Tetramethyl guanidine (TMG, Aladdin, 99%) was dried using KOH before its use. Dimethyl sulfoxide (DMSO, Kermel Reagents, AR) was dried using 4 Å molecular sieves before use. Sodium borohydride ($NaBH_4$, 98%) was purchased from Kermel Reagents Co., Ltd (Tianjin, China). Succinic anhydride (SA, Aladdin, 99%), pyromellitic dianhydride (PMDA, Aladdin, 99%), α-angelica lactone (α-AL, Aladdin, >95%), γ-valerolactone (GVL, Aladdin, 98%), 1-hexene (Aladdin, 99%), cyclohexene (Aladdin, 98%) and palladium chloride ($PdCl_2$, Aladdin, 59%–60%) were directly used without any additional chemical treatment. Carbon dioxide (CO_2, purity: >99.999%) was supplied by Guiyang Sanhe Gas Co., Ltd (Guizhou, China). Styrene (SE, 99.5%) was purchased from Energy Chemical Co., Ltd (Shanghai, China).

Preparation of CPILH

The preparation of the cotton pulp cellulose solution followed a previously published method.[30] Initially, 1 g of cotton pulp cellulose was suspended in a customized high-pressure autoclave containing a mixture of TMG (2.15 g) and DMSO (29.36 g). The autoclave was then purged with CO_2 three times to remove air and pressurized with CO_2 to 1 MPa. Subsequently, the autoclave was placed in an oil bath at 50 °C and stirred magnetically for 3 h, resulting in a clear 3 wt% cellulose solution. Next, a solution of SA (0.561 g, n_{AGU}/n_{SA} = 1/1, DMSO) was added to 30 g of the 3 wt% cellulose solution, and the mixture was vigorously stirred and reacted at 80 °C for 3 h. Following this, PMDA (1.224 g, n_{AGU}/n_{PMDA} = 1/1, DMSO) was slowly added to the mixture while vigorously stirring in an ice/water bath, ensuring the formation of a homogeneous solution. The resulting homogeneous solution was then poured into a round culture dish with a diameter of 12 cm and stored at 80 °C for 5 h to obtain a CPILH precursor. Finally, the CPILH precursor was shaped into cylinders using a puncher with a diameter of 5 mm. The resulting cylinders were washed with deionized water for two days to remove excess DMSO.

Preparation of the Pd@CPILH catalyst

CPILH discs fully absorb the solute in $PdCl_2$ aqueous solution (100 mL, 0.1 mg mL^{-1}) with continuous vibration using a water bath shaker for 24 h (150 rpm). The resulting gels were then transferred to deionized water for an additional 24 h, resulting in the formation of yellow Pd^{2+}@CPILH gels. Subsequently, the Pd^{2+}@CPILH gels were immersed in 100 mL of 0.1 mol L^{-1} $NaBH_4$ aqueous solutions for 12 h, followed by soaking in deionized water for another 12 h to obtain the

Pd@CPILH hydrogel catalyst. It is worth noting that in the catalytic process, when Pd@CPILH catalyzes hydrogenation of α-AL in ethanol, methanol and THF, the Pd@CPILH hydrogel catalyst undergoes a complete replacement of the water with ethanol, methanol and THF, respectively.

Characterization

The Fourier transform infrared (ATR-FTIR) spectra were recorded using a Nicolet iS5 instrument from USA. X-ray diffraction (XRD) spectra were obtained using a PANalytical X'pert Advance X-ray diffractometer with Cu Kα radiation (λ = 1.54 Å) operating at 40 kV and 40 mA. XPS analysis was performed using a Thermo Scientific K-Alpha X-ray photoelectron spectroscopy analyzer equipped with AI Kα radiation. Samples were characterized using a Tecnai G2 F20 (FEI, Czech Republic) field emission transmission electron microscope (TEM) for imaging. Detailed structural analysis was conducted using high-resolution TEM (HRTEM), while selected area electron diffraction (SAED) provided crystallographic information. Elemental composition analysis was carried out using energy-dispersive X-ray spectroscopy (EDX). The mass fraction of Pd in the samples was determined using an Agilent 5110 plasma emission spectrometer. To prepare the samples for testing, the freeze-dried sample was dissolved in aqua regia and then diluted tenfold before analysis. The amount of Pd NPs adsorbed in the hydrogel beads was determined using Thermo Fisher iCAP 740 ICP-OES. Prior to determination, the solid samples were treated by acid digestion assisted by microwave irradiation using aqua regia.

Catalytic hydrogenation of α-AL

In a 50 mL round-bottom flask, solutions of α-AL (20 mg) in 10 mL of different solvent systems (*e.g.*, water, ethanol, methanol and THF) were prepared, respectively. After replacing with H_2 gas three times, the reaction system is placed in an oil bath at 30 °C under a certain H_2 atmosphere and stirring for a certain period of time. A gas chromatograph (GC, EWAI GC-4100) equipped with a 0.32 mm × 50 m KB-5 capillary column and N_2 as the carrier gas were employed to analyze and identify the catalytic reaction products. For recycling purposes, Pd@CPILH catalysts were separated by filtration, cleaned with water, ethanol, methanol and THF, respectively, and subsequently added to fresh reactant for the next catalytic reaction.

The reaction rate constant can be given by eqn (1):

$$\ln(C_{\alpha\text{-AL}}) = kt \quad (1)$$

$C_{\alpha\text{-AL}}$ is the concentration of α-AL, t is the reaction time, and k is the rate constant.

The activation energy (E_a) was calculated using the Arrhenius eqn (2):

$$k = Ae^{-E_a/RT} \quad (2)$$

E_a is the activation energy, A is the pre-exponential factor, R is the ideal gas constant, and T is the temperature (expressed in K).

Results and discussion

Preparation and characterization of CPILH and Pd@CPILH

The cotton pulp cellulose was successfully dissolved in TMG/CO_2/DMSO.[31–33] In this process, a specific molar ratio of two types of cyclic anhydride (SA and PMDA) was added to the cellulose solution (3 wt%) to achieve the CPILH through chemical cross-linking without an external catalyst (Fig. 1a and b). In this system, the presence of TMG facilitates the interaction between TMG and the hydroxyl groups in cellulose. This interaction enhances the nucleophilicity of the hydroxyl groups, enabling them to undergo a nucleophilic attack at the carbonyl groups in SA and PMDA. Consequently, this leads to the ring opening of SA and PMDA, resulting in the formation of a cellulose ester structure through an acylation mechanism.[29] According to our previous report, an appropriate amount of PMDA (a dianhydride, acting as a cross-linker) contributes to the successful preparation and property adjustability of the CPILH.[30] Thus, in this study, the CPILH was finally designed with a molar ratio of SA to AGU of 1 : 1 and PMDA to AGU of 1 : 1. With the prepared CPILH in hand, the Pd@CPILH catalyst was achieved by immersing the CPILH in $PdCl_2$ aqueous solution to adsorb Pd^{2+} followed by $NaBH_4$ treatment to reduce Pd^{2+} to Pd NPs. Thus, it is believed that TMG plays multiple roles in the preparation of CPILH and Pd@CPILH: (1) an essential component for successful cellulose dissolution; (2) an effective *in situ* organic catalyst for acylation of cellulose with SA and PMDA to form a gel matrix; (3) a cationic moiety for the construction of CPILH; and (4) anchoring sites for stabilizing Pd NPs.

FTIR measurements were conducted to analyze the chemical structure of CPILH and Pd@CPILH, as illustrated in Fig. 2a. In general, the broad peak observed in the range of 3600–3100 cm^{-1} corresponds to the –OH stretching vibration of the hydroxyl groups present in cellulose. The peak at 1725 cm^{-1} is attributed to the stretching vibration of ester groups (C=O), while the peaks at 1650 cm^{-1} and 1566 cm^{-1} are attributed to the stretching vibrations of the terminal ester group (C=O) and TMG (C=N), respectively.[34,35] Additionally, the bands observed at 1391 cm^{-1} and 1252 cm^{-1} are indicative of the stretching vibrations of methylene groups within the succinic acid chain.[36] These results indicate that an acylation reaction occurred between cellulose and either SA or PMDA. For Pd@CPILH, the spectrum is almost the same as CPILH, demonstrating a nearly unchanged chemical structure of the gel matrix in the adsorption and reduction processes. The XRD diffraction patterns of CPILH and Pd@CPILH exhibit similar patterns, with the exception of a distinct diffraction peak at 39° corresponding to the (111) crystal plane of Pd NPs in the Pd@CPILH sample (Fig. 2b). This peak provides strong evidence for the incorporation and retention of Pd NPs within the CPILH structure.[37]

The TEM images reveal that the Pd NPs are evenly distributed within the CPILH matrix, displaying no significant agglomeration (Fig. 2e). The average size of the Pd NPs is about 4.4 nm (Fig. 2c). The high-resolution transmission electron

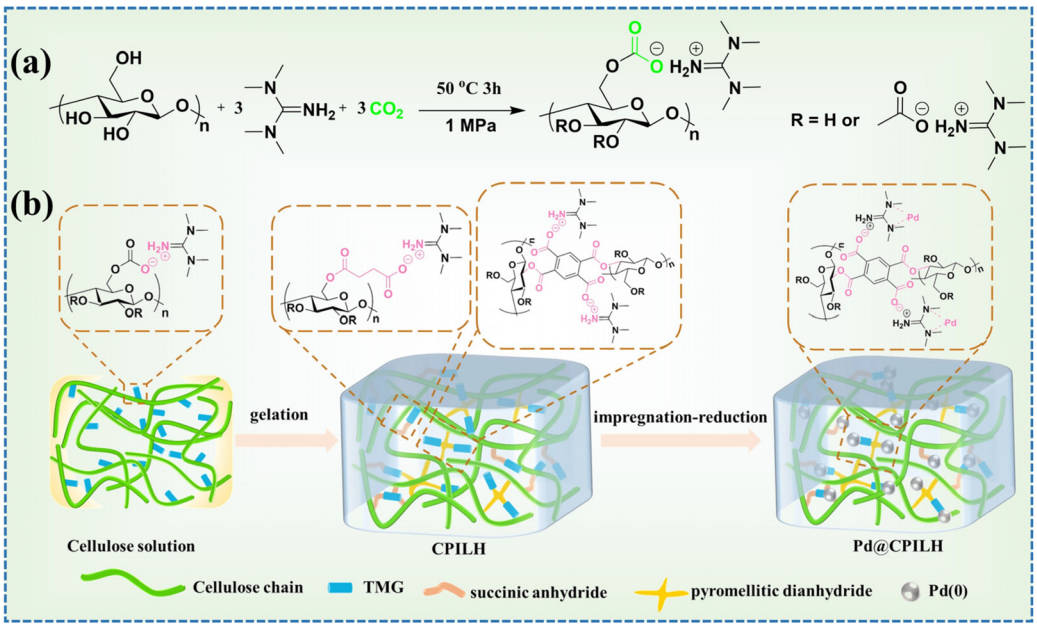

Fig. 1 The synthesis of CPILH and the Pd@CPILH catalyst. (a) Dissolution of cellulose in the TMG/CO_2/DMSO solvent system. (b) Schematic diagram of the preparation of CPILH and Pd@CPILH.

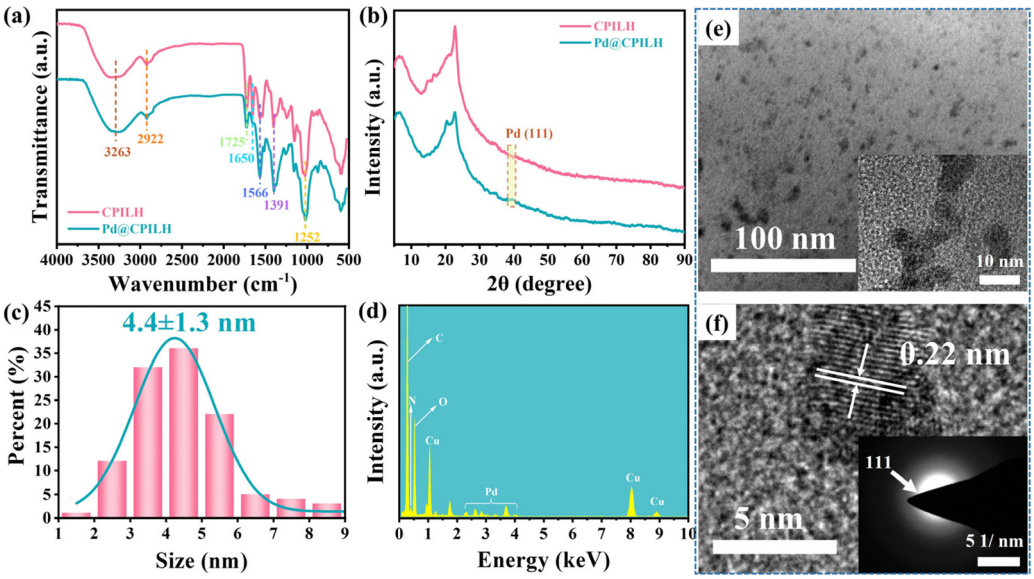

Fig. 2 (a) FTIR spectra and (b) XRD patterns of CPILH and Pd@CPILH. (c) Size distribution, (d) EDX result, (e) TEM, and (f) HRTEM and SAED of Pd@CPILH.

microscopy (HRTEM) image exhibits a lattice fringe in Pd NPs with a distance of 0.22 nm, indicating the presence of (111) planes (Fig. 2f).[37] In addition, the SAED image displays a diffraction ring, indicating the polycrystalline nature of the Pd crystals.[38] The EDX result of Pd@CPILH also demonstrates the existence of the Pd element (Fig. 2d). The even distribution of Pd NPs within the CPILH matrix can be attributed to the exceptional coordination ability of guanidine moieties, along with the presence of hydroxyl and carboxyl groups in CPILH, which facilitate the interaction with Pd NPs. Additionally, the loading amount of Pd in CPILH was assessed using inductively coupled plasma optical emission spectroscopy (ICP-OES), which determined a loading capacity of 1.6 wt% of Pd NPs.

XPS measurement was further conducted to investigate the chemical state of elements in CPILH and Pd@CPILH. The survey spectrum of CPILH exclusively indicates the presence of C, O, and N, while Pd@CPILH contains C, O, N, and Pd (Fig. 3a), implying the effective incorporation of Pd NPs by

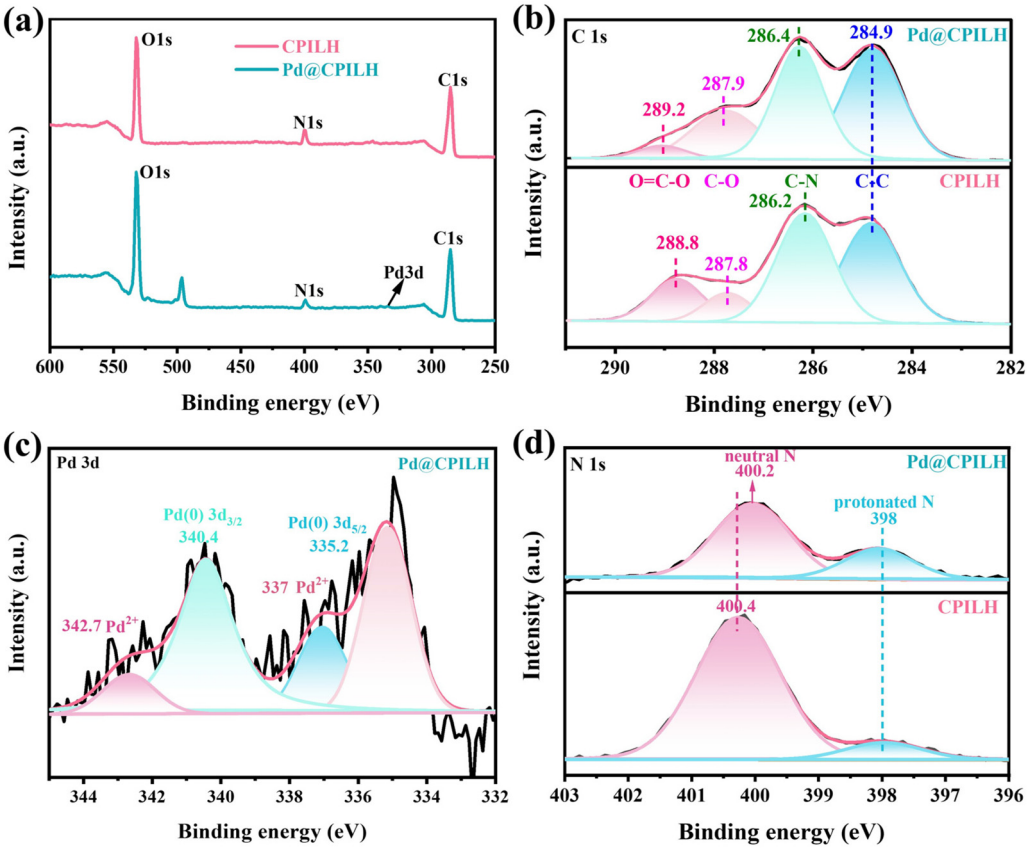

Fig. 3 XPS spectra of CPILH and Pd@CPILH: (a) survey, (b) high-resolution spectra of C 1s, (c) high-resolution spectrum of Pd 3d, and (d) high-resolution spectra of N 1s.

CPILH. The XPS peaks for the C 1s spectrum of the support CPILH were fitted and found to be centered at 284.9, 286.2, 287.8, and 288.8 eV (Fig. 3b). These peaks can be ascribed to the presence of C–C, C–N, C–O, and O–C=O covalent bonds, respectively. In comparison with the C 1s spectra of CPILH, the peaks associated with C–N, C–O, and O=C–O in the Pd@CPILH catalyst exhibit a slight shift towards higher binding energies. This shift suggests a partial transfer of electrons from the C–N, C–O, and O=C–O bonds to the Pd species in the catalyst.[39]

The high-resolution spectrum of Pd in the Pd@CPILH catalyst reveals two distinct sets of peaks correlating to Pd $3d_{5/2}$ and Pd $3d_{3/2}$ (Fig. 3c). This observation indicates the presence of both zero-valence palladium (Pd^0) and two-valence palladium (Pd^{2+}) in the catalyst.[40] Specifically, the Pd $3d_{5/2}$ and Pd $3d_{3/2}$ peaks at 335.2 and 340.4 eV are associated with Pd^0, while the peaks at 337 eV and 342.7 eV are attributed to Pd^{2+} in Pd $3d_{5/2}$ and Pd $3d_{3/2}$, respectively.[41] Their content of Pd^0 and Pd^{2+} in the Pd@CPILH catalyst can be calculated to be 76.7% and 23.3%, respectively.[30] The predominant state of palladium in CPILH is Pd^0, with some residual Pd^{2+} present in the catalyst. This observation suggests that the presence of Pd^{2+} could be attributed to the strong electrostatic interaction between the carboxyl or hydroxyl group and Pd^{2+}. Furthermore, the N 1s spectrum of CPILH (Fig. 3d) exhibits two distinct types of N species. The peaks detected at 400.4 and 398 eV can be ascribed to neutral nitrogen (N–C) and protonated nitrogen (N–H) of TMG moieties, respectively.[42] After anchoring Pd nanoparticles, the binding energy of N–C decreased from 400.4 eV to 400.2 eV. This decrease can be ascribed to electron transfer from N to Pd. On the other hand, the binding energy of protonated N remained nearly unchanged in Pd@CPILH, indicating that the dominant anchoring sites for Pd NPs are the neutral nitrogen in TMG cationic moieties.

Selective hydrogenation of α-AL by the Pd@CPILH catalyst

The catalytic performance of the Pd@CPILH catalyst was evaluated under mild conditions using the hydrogenation of α-AL to GVL as a model reaction. The GC spectrum of the standard α-AL solution shows that α-AL partially isomerizes to β-AL, which is consistent with a previous report (Fig. 4a).[43] To quantify the conversion from α-AL to GVL, the calibration curve of α-AL was determined to be $y = 48\,133.24517x$ ($R^2 = 0.998$), where x and y are the concentration of α-AL and the corresponding peak area, respectively. It is obvious that the peak area is linear with the concentration of α-AL, indicating that the isomerization of α-AL to β-AL has negligible influence on the quantification of α-AL by GC technology. After hydrogenation for 2 h catalyzed by Pd@CPILH, the signal of GVL

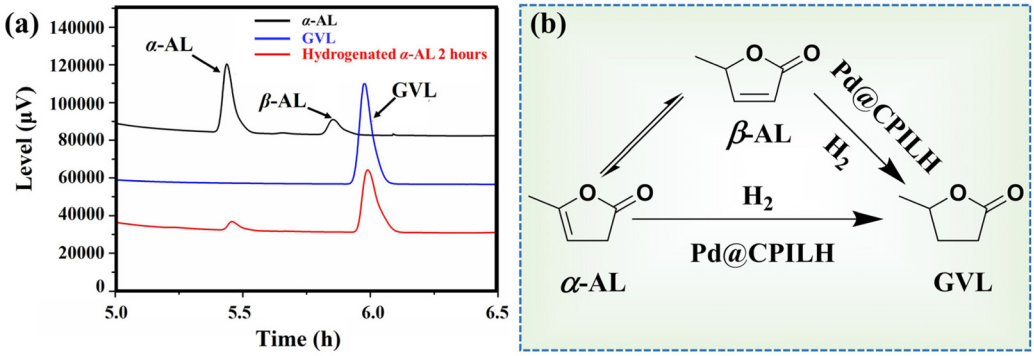

Fig. 4 (a) GC curves of α-AL, GVL, and the reaction solution after hydrogenation for 2 h catalyzed by Pd@CPILH. (b) Predictive route of α-AL hydrogenation.

appeared while β-AL vanished. Therefore, two possible pathways for hydrogenation of α-AL can be deduced. Firstly, α-AL may be unstable and partially isomerize to β-AL, which is then hydrogenated to GVL by the catalyst.[21] Secondly, α-AL may be hydrogenated directly into GVL (Fig. 4b).[44] A similar hydrogenation mechanism of α-AL to GVL has been proposed by Vries *et al.*[43] That is, in the initial stage of the hydrogenation α-AL reaction, only isomerized β-AL is produced due to the lack of a hydrogen source. However, in the presence of a hydrogen source, both α-AL and β-AL are hydrogenated to GVL. In this regard, it is highly desirable to explain the mechanism for the hydrogenation of α-AL to GVL.

Firstly, four frequently used solvents (*i.e.*, CH_3CH_2OH, CH_3OH, water, and THF) were employed to reveal the influence of solvents on the hydrogenation of α-AL. The catalytic performance of Pd@CPILH in ethanol resulted in the highest conversion efficiency of α-AL (92.2%) after a 2 h hydrogenation reaction at 50 °C. Adversely, Pd@CPILH in THF exhibited the lowest conversion efficiency (only 1.6%). This indicates that the choice of solvent significantly affects the catalytic performance. On the one hand, this may be due to the varying solubility in different solvents (Fig. 5a).[45] On the other hand, the Pd@CPILH catalyst undergoing different solvent substitutions may undergo phase separation, which affects the morphology of the Pd@CPILH catalyst and may ultimately affect the catalytic performance. To exclude the impact of the substrate material on the catalytic activity, CPILH was used as a catalyst in ethanol showing no catalytic activity. Therefore, ethanol was chosen as the solvent for further investigation.

With the extension of the reaction time, the conversion of α-AL gradually increased, indicating that a longer reaction time can make α-AL more completely converted to the target

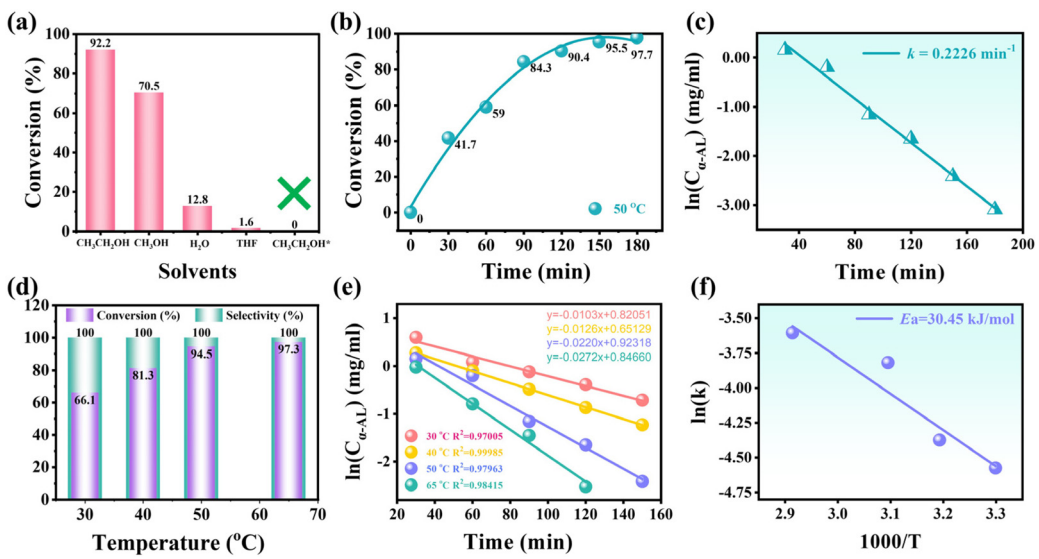

Fig. 5 Effect of (a) solvents and (b) the reaction time on the hydrogenation of α-AL to GVL at 50 °C. (c) First-order kinetics for α-AL hydrogenation by using ethanol as a solvent at 50 °C. (d) Effect of temperature on the hydrogenation of α-AL by the Pd@CPILH catalyst. (e) α-AL concentration over time profiles at various temperatures. (f) Temperature dependence of rate constants. Experimental conditions: α-angelica (20 mg), Pd@CPILH (20 mg), solvent (10 mL), CH_3CH_2OH* represents CPILH as a catalyst in CH_3CH_2OH (20 mg).

product (Fig. 5b). During the reaction, a conversion rate of 41.6% was observed after 30 minutes, indicating that a significant portion of α-AL had been converted. After 90 minutes, the conversion rate increased to 84.3%, indicating further progress in the hydrogenation reaction. After prolonging the reaction time to 3 h, a conversion of 97.7% was achieved. Turnover frequency (TOF) serves as a critical metric for assessing the catalytic activity of catalysts. It is calculated by dividing the concentration of converted α-AL (mole) by the amount of noble metal used as the catalyst (mole) and the reaction time (h). The TOF of Pd@CPILH in the hydrogenation of α-AL reached 56.4 h^{-1}, significantly surpassing that of Pd-NiO/SiO_2.[23] The kinetics of α-AL hydrogenation to GVL were also investigated, revealing a linear correlation between $\ln(C_{\alpha\text{-AL}})$ and time (Fig. 5c). The reaction rate constant (k) determined using eqn (1) was 0.2226 min^{-1}, indicating that the hydrogenation of α-AL to GVL catalyzed by Pd@CPILH conforms to a first-order kinetic model.

To elucidate the thermodynamic process of α-AL hydrogenation, the impact of temperature on the reaction was investigated. Employing the Pd@CPILH catalyst, the catalytic hydrogenation of α-AL to GVL displayed a pronounced temperature dependence (Fig. 5d). As the reaction temperature rose from 30 °C to 65 °C, the conversion of α-AL escalated from 66.1% to 97.3%, with complete selectivity achieved after 3 h. This may be due to the fact that the catalytic hydrogenation of α-AL is thermodynamically favorable, and the increase of temperature is more conducive to mass transfer, thereby improving the catalytic activity of α-AL hydrogenation.[46] Meanwhile, the k values at 30, 40, 50, and 65 °C are determined to be 0.0103, 0.0126, 0.0220, and 0.0272 min^{-1}, respectively (Fig. 5e). The E_a of the reaction catalyzed by Pd@CPILH was determined by

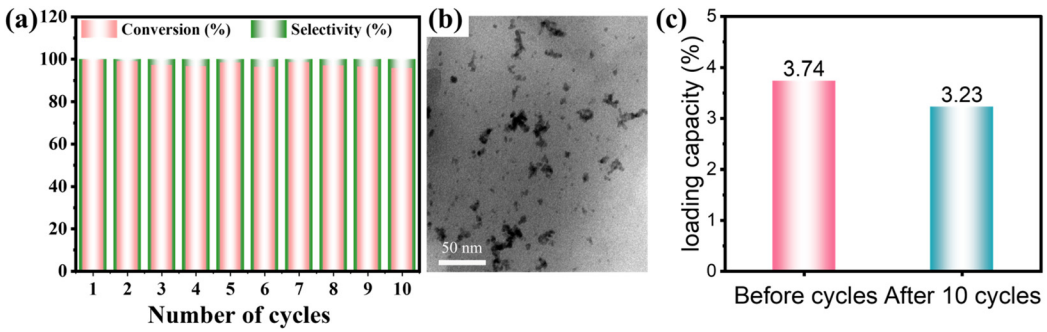

Fig. 6 (a) Recycling stability of α-AL hydrogenation and (b) TEM image for Pd@CPILH after recycling experiments. (c) Comparison of Pd NP loading capacity before and after catalysis.

Table 1 Pd@CPILH catalyzed alkene hydrogenation[a] and comparison with reported works

Catalyst	Alkene	Product	Solvent	Time (h)	Temperature (°C)	Conv.[b] (%)	Sel.[b] (%)	Ref.
Pd@CPILH			Ethanol	3.5	30	100	99.9	This work
			Ethanol	2.5	30	100	99.9	
			Ethanol	3	30	100	99.9	
Pd/ZIF-8			Ethyl acetate	24	30	Nearly 100	—	47
Pd-PEG2000			PEG2000[c]	2.75	70	99	100	48
Pd-Phenanthroline			PEG[c]	8	30	44	100	49
Pd@ZIF-8			Methanol	—	40	47	54	50
Pd@MOF-5			—	12	35	>99.7	—	51
Pd/g-C_3N_4			Ethanol	18	25	>95	—	52
Pd-Phenanthroline			PEG[c]	4	50	100	100	49
Pd-PEG2000			PEG2000[c]	0.25	70	100	100	48
Pd-PEG2000			PEG2000[c]	1.33	70	100	100	48
Pd-Phenanthroline			PEG[c]	20	40	50	100	49

[a] Conditions: alkenes (20 mg), cat. Pd@CPILH (20 mg, Pd NPs content of 1.6 wt%), ethanol (10 mL). [b] Conv. (%) and sel. (%) were determined by GC. [c] Polyethylene glycol abbreviated as PEG.

employing the Arrhenius eqn (2), which yielded a value of 30.45 kJ mol^{-1} for the hydrogenation of α-AL using the Pd@CPILH catalyst (Fig. 5f). In general, the apparent activation energy can be used to determine the processes that affect chemical reactions. The activation energy of the reaction process controlled by diffusion in solution reactions is lower (8–21 kJ mol^{-1}), while the activation energy of the reaction process controlled by surface processes is higher (>29 kJ mol^{-1}). Thus, it can be seen that the catalytic hydrogenation reaction of α-AL to GVL is controlled by surface processes.

Recycling stability of the Pd@CPILH catalyst

The investigation of the recycling stability of the Pd@CPILH catalyst was conducted to evaluate its performance over multiple cycles, which is an essential parameter from a practical perspective. After subjecting the Pd@CPILH catalyst to 10 cycles, the conversion of α-AL consistently remained at 93%, while the selectivity remained approximately 100% (Fig. 6a). Moreover, the dispersion of Pd NPs in Pd@CPILH remains uniform with a slightly bigger size distribution (Fig. 6b). The loading of Pd NPs in the Pd@CPILH catalyst was further evaluated by ICP-OES. The results show that the initial loading of Pd NPs is 3.74%, and the loading after 10 cycles is 3.23%, and only 0.051% loading decrease per cycle occurs, indicating that there will be no serious leaching and deactivation in the long-term catalytic process (Fig. 6c).

Selective hydrogenation of alkenes by the Pd@CPILH catalyst

To investigate the applicability of the Pd@CPILH catalyst for the selective hydrogenation of other types of alkenes, styrene, 1-hexene, and cyclohexene were selected as reactants for the hydrogenation reaction by the Pd@CPILH catalyst. As shown in Table 1, the three kinds of alkenes can be completely transformed into the corresponding products at 30 °C after 2.5 h, 3.5 h, and 3 h, respectively, with a selectivity of 99.9%. These results show that the hydrogenation of alkenes catalyzed by Pd@CPILH can reach 100% under mild conditions with high selectivity. As presented in Table 1, compared with other catalysts, the Pd@CPILH catalyst achieves a higher conversion for the hydrogenation of the three alkenes.[47–52]

Conclusions

In summary, by harnessing the versatility of the TMG component, two cyclic anhydrides were introduced into a cellulose/TMG/CO_2/DMSO solution, resulting in the straightforward synthesis of a cellulose gel containing TMGPIL through esterification. TMG plays multiple roles in the preparation of CPILH and Pd@CPILH: (1) an essential component for successful cellulose dissolution; (2) an effective *in situ* organic catalyst for acylation of cellulose with SA and PMDA to form a gel matrix; (3) a cationic moiety for the construction of CPILH; and (4) anchoring sites for the subsequent supporting and stabilizing Pd NPs. The investigation revealed that the Pd NPs exhibited a homogeneous dispersion within the gel matrix, characterized by a small size of 4.4 nm. The Pd@CPILH catalyst exhibited the desired catalytic hydrogenation of α-AL to GVL, achieving a high conversion rate of 97.7% and complete selectivity within a 3 h reaction time at 50 °C in ethanol. The reaction rate constant k is determined to be 0.2226 min^{-1} at 50 °C, and the E_a is calculated to be 30.45 kJ mol^{-1}. The as-prepared Pd@CPILH catalyst exhibited excellent recyclability, as there was no significant deterioration observed in both conversion and selectivity even after 10 successive uses. Furthermore, the Pd@CPILH catalyst also demonstrated exceptional catalytic efficiency of common alkenes. From the perspective of material construction, the use of biomass cotton as a raw material to react skillfully with SA and PMDA is a typical atom economical reaction without any by-products. From the solvent point of view, the use of TMG and DMSO does cause environmental concerns, so the recycling of TMG and DMSO is a focus of our group's future work. In a word, the Pd@CPILH catalyst has potential applications in the future in a variety of sectors including smart materials, medicinal materials, and green catalysis.

Data availability

The authors confirm that the data supporting the findings of this study are available within the article and its ESI.

Conflicts of interest

There are no conflicts to declare.

Acknowledgements

This work was supported by the National Natural Science Foundation of China (22275041; 21574030); Science and Technology Department of Guizhou Province (Natural Science Key Fund ZK [2021]023); Guizhou Province Basic Research Program (Natural Science ZK [2024]078); Specific Natural Science Foundation of Guizhou University (X2022009); Graduate Student Innovation Research Fund of Guizhou Province, China [YJSKYJJ(2021)201].

References

1 G. Sirasani, L. Tong and E. P. Balskus, *Angew. Chem., Int. Ed.*, 2014, **53**, 7785–7788.
2 S. Guo, X. Wang and J. S. Zhou, *Org. Lett.*, 2020, **22**, 1204–1207.
3 J. Q. Bond, D. M. Alonso, D. Wang, R. M. West and J. A. Dumesic, *Science*, 2010, **327**, 1110–1114.
4 D. M. Alonso, S. G. Wettstein, M. A. Mellmer, E. I. Gurbuz and J. A. Dumesic, *Energy Environ. Sci.*, 2013, **6**, 76–80.
5 A. Kumar, Y. E. Jad, J. M. Collins, F. Albericio and B. G. D. L. Torre, *ACS Sustainable Chem. Eng.*, 2018, **6**, 8034–8039.

6 I. Anastasiou, F. Ferlin, O. Viteritti, S. Santoro and L. Vaccaro, *Mol. Catal.*, 2021, **513**, 111787–111793.
7 X. Shen, D. Xia, Y. Xiang and J. Gao, *e-Polym.*, 2019, **19**, 323–329.
8 F. Valentini, G. Brufani, B. D. Erasmo and L. Vaccaro, *Curr. Opin. Green Sustainable Chem.*, 2022, **36**, 100634–100641.
9 L. Ye, Y. Han, J. Feng and X. Lu, *Ind. Crops Prod.*, 2019, **144**, 112031–112046.
10 M. Chen, Q. Ma, J. Y. Zhu, D. M. Alonsod and T. Runge, *Green Chem.*, 2019, **21**, 5316–5325.
11 D. M. Alonso, S. G. Wettstein and J. A. Dumesic, *Green Chem.*, 2013, **15**, 584–595.
12 V. Molinari, M. Antonietti and D. Esposito, *Catal. Sci. Technol.*, 2014, **4**, 3626–3630.
13 X. Huang, S. Kudo, U. P. M. Ashik, H. Einaga and J.-I. Hayashi, *Energy Fuels*, 2020, **34**, 7190–7197.
14 S. Choi, C. W. Song, J. H. Shin and S. Y. Lee, *Metab. Eng.*, 2015, **28**, 223–239.
15 A. M. R. Galletti, C. Antonetti, V. De Luise and M. Martinelli, *Green Chem.*, 2012, **14**, 688–694.
16 P. Gallezot, *Chem. Soc. Rev.*, 2012, **41**, 1538–1558.
17 F. M. Geilen, B. Engendahl, A. Harwardt, W. Marquardt, J. Klankermayer and W. Leitner, *Angew. Chem.*, 2010, **122**, 5642–5646.
18 J. P. Lange, J. Z. Vestering and R. J. Haan, *Chem. Commun.*, 2007, **33**, 3488–3490.
19 P. Zhang, Q. Yuan, L. Chen, T. Xue, Y. Guan and P. Wu, *RSC Adv.*, 2016, **6**, 65377–65382.
20 M. M. Antunes, A. F. Silva, A. Fernandes and A. A. Valente, *Catal. Today*, 2022, **394**, 268–281.
21 R. Cao, J. Xin, Z. Zhang, Z. Liu, X. Lu, B. Ren and S. Zhang, *ACS Sustainable Chem. Eng.*, 2014, **2**, 902–909.
22 M. M. Antunes, A. F. Silva, A. Fernandes and A. A. Valente, *Catal. Today*, 2022, **394–396**, 268–281.
23 P. Zhang, Q. Yuan, L. Chen, T. Xue, Y. Guan and P. Wu, *RSC Adv.*, 2016, **6**, 65377–65382.
24 P. Zhang, C.-H. Liu, L. Chen, J.-M. Chen, Y. Guan and P. Wu, *J. Catal.*, 2017, **351**, 10–18.
25 L. C. Wong, C. P. Leh and C. F. Goh, *Carbohydr. Polym.*, 2021, **264**, 118036.
26 P. Zugenmaier, *Carbohydr. Polym.*, 2020, **254**, 117417–117433.
27 W. Zhou, M. Chen, Q. Tian, J. Chen, X. Xu and C.-P. Wong, *Energy Storage Mater.*, 2022, **44**, 57–65.
28 W. Peng, Y. Yan, D. Zhang, Y. Zhou, D. Na, C. Xiao, C. Yang, G. Wen and J. Zhang, *Colloids Surf., A*, 2021, **624**, 126809.
29 X. Zhu, L. Zhang, G. Zou, Q. Chen, Y. Guo, S. Liang, M. North and H. Xie, *Int. J. Biol. Macromol.*, 2021, **180**, 792–803.
30 X. Li, F. Dong, L. Zhang, Q. Xu, X. Zhu, S. Liang, L. Hu and H. Xie, *Chem. Eng. J.*, 2019, **372**, 516–525.
31 H. Xie, X. Yu, Y. Yang and Z. K. Zhao, *Green Chem.*, 2014, **16**, 2422–2427.
32 J. Gan, Y. Peng, Q. Chen, G. Hu, Q. Xu, L. Jin and H. Xie, *Bioresour. Technol.*, 2020, **295**, 122230–122237.
33 X. Li, Q. Xu, H. Shen, Y. Guo, M. Wu, Y. Peng, L. Zhang, Z. K. Zhao, Y. Liu and H. Xie, *Carbohydr. Polym.*, 2019, 50–58, DOI: 10.1016/j.carbpol.2018.09.085.
34 T. Yoshimura, K. Matsuo and R. Fujioka, *J. Appl. Polym. Sci.*, 2006, **99**, 3251–3256.
35 X. Sang, C. Qin, Z. Tong, S. Kong, Z. Jia, G. Wan and X. Liu, *Cellulose*, 2017, **24**, 2415–2425.
36 P. I. Omwene, Z. B. O. Sarihan, A. Karagunduz and B. Keskinler, *Food Bioprod. Process.*, 2021, **129**, 1–9.
37 P. Han, C. Tang, S. Sarina, E. R. Waclawik, A. Du, S. E. Bottle, Y. Fang, Y. Huang, K. Li and H. Y. Zhu, *ACS Catal.*, 2022, **12**, 2280–2289.
38 M. Maity and U. Maitra, *J. Mater. Chem. A*, 2014, **2**, 18952–18958.
39 M. Zhang, Y. Liu, H. Zhao, J. Tao, N. Geng, W. Li and Y. Zhai, *ACS Appl. Mater. Interfaces*, 2021, **13**, 19904–19914.
40 J. Li, L. Zhong, L. Tong, Y. Yu, Q. Liu, S. Zhang, S. Li, R. Si and J. Zhang, *Adv. Funct. Mater.*, 2019, **29**, 1905423.
41 X. Tan, J. Qin, Y. Li, Y. Zeng and H. Li, *J. Hazard. Mater.*, 2020, **397**, 122786.
42 Y. Dong, J. Bi, S. Ming, S. Zhang, D. Zhu, D. Meng and T. Li, *Carbohydr. Polym.*, 2021, **260**, 117815–117824.
43 F. E. Ouahabi, W. Smit, C. Angelici, M. Polyakov, U. Rodemerck, C. Fischer, V. N. Kalevaru, S. Wohlrab, S. Tin, G. P. M. V. Klink, J. C. V. D. Waal, F. O. Orange and J. G. D. Vries, *ACS Sustainable Chem. Eng.*, 2022, **10**, 66–775.
44 T. Raj, K. Chandrasekhar, R. Banu, J.-J. Yoon, G. Kumar and S.-H. Kim, *Fuel*, 2021, **303**, 121333–121347.
45 S. Maki, Y. Harada, R. Matsui, M. Okawa, T. Hirano, H. Niwa, M. Koizumi, Y. Nishiki, T. Furuta, H. Inoue and C. Iwakura, *Tetrahedron Lett.*, 2001, **42**, 8323–8327.
46 W. Wang, R. Wang, X. Jiang, Z.-H. He, K. Wang, Y. Yang and Z.-T. Liu, *Appl. Catal., A*, 2022, **634**, 118537.
47 H. Yin, J. Choi and A. C. K. Yip, *Catal. Today*, 2016, **265**, 203–209.
48 X. Ma, J. Tao, B. Han, J. Zhang, S. Miao, K. Ding, G. An, X. Ye, Y. Zhou and A. Zhu, *Catal. Commun.*, 2008, **9**, 70–74.
49 U. R. Pillai and E. Sahle-Demessie, *J. Mol. Catal. A: Chem.*, 2004, **222**, 153–158.
50 N. Gholampour, S. Chaemchuen, Z.-Y. Hu, B. Mousavi, G. V. Tendeloo and F. Verpoort, *Chem. Eng. J.*, 2017, **322**, 702–709.
51 M. Sabo, A. Henschel, H. Frde, E. Klemm and S. Kaskel, *J. Mater. Chem.*, 2007, **17**, 3827–3832.
52 C. Han, P. Meng, E. Waclawik, C. Zhang, X.-H. Li, H. Yang, M. Antonietti and J. Xu, *Angew. Chem., Int. Ed.*, 2018, **57**, 14857–14861.